Atmospheric
Chemistry
and Physics
Discussions

Open Access

Global temperature response to the major volcanic eruptions in multiple reanalysis datasets

M. Fujiwara[1], T. Hibino[1,*], S. K. Mehta[2,**], L. Gray[3], D. Mitchell[3], and J. Anstey[3]

[1]Graduate School of Environmental Science, Hokkaido University, Sapporo, Japan
[2]Research Institute for Sustainable Humanosphere, Kyoto University, Uji, Japan
[3]Atmospheric, Oceanic and Planetary Physics, University of Oxford, Oxford, UK
[*]now at: PAP Corporation, Nagoya, Japan
[**]now at: Research Institute, SRM University, Chennai, India

Correspondence to: M. Fujiwara (fuji@ees.hokudai.ac.jp)

ACPD

15, 13315–13346, 2015

Response to volcanic eruptions in reanalyses

M. Fujiwara et al.

Title Page

Abstract	Introduction
Conclusions	References
Tables	Figures

|◀ | ▶|

◀ | ▶

Back | Close

Full Screen / Esc

Printer-friendly Version

Interactive Discussion

Full Screen / Esc

Printer-friendly Version

Interactive Discussion

Abstract

Global temperature response to the eruptions of Mount Agung in 1963, El Chichón in 1982 and Mount Pinatubo in 1991 is investigated using nine reanalysis datasets (JRA-55, MERRA, ERA-Interim, NCEP-CFSR, JRA-25, ERA-40, NCEP-1, NCEP-2, and 20CR). Multiple linear regression is applied to the zonal and monthly mean time series of temperature for two periods, 1979–2009 (for eight reanalysis datasets) and 1958–2001 (for four reanalysis datasets), by considering explanatory factors of seasonal harmonics, linear trends, Quasi-Biennial Oscillation, solar cycle, and El Niño Southern Oscillation. The residuals are used to define the volcanic signals for the three eruptions separately. In response to the Mount Pinatubo eruption, most reanalysis datasets show strong warming signals (up to 2–3 K for one-year average) in the tropical lower stratosphere and weak cooling signals (down to −1 K) in the subtropical upper troposphere. For the El Chichón eruption, warming signals in the tropical lower stratosphere are somewhat smaller than those for the Mount Pinatubo eruption. The response to the Mount Agung eruption is asymmetric about the equator with strong warming in the Southern Hemisphere midlatitude upper troposphere to lower stratosphere. The response to three other smaller-scale eruptions in the 1960s and 1970s is also investigated. Comparison of the results from several different reanalysis datasets confirms the atmospheric temperature response to these major eruptions qualitatively, but also shows quantitative differences even among the most recent reanalysis datasets.

1 Introduction

Explosive volcanic eruptions inject sulphur species to the stratosphere in the form of SO_2 and H_2S which convert to H_2SO_4 aerosols. These aerosols are then transported both vertically and horizontally into the stratosphere by the Brewer–Dobson circulation (Butchart, 2014), stay there to perturb the radiative budget on a timescale of a few

years, and thus affect global climate (Robock, 2000). The stratospheric volcanic aerosol layer is heated by absorption of near-infrared solar radiation and upward longwave radiation from the troposphere and surface. In the troposphere, the reduced near-infrared solar radiation is compensated by the additional downward longwave radiation from the aerosol layer. At the surface, large reduction in direct shortwave radiation due to the aerosol layer mainly contributes to net cooling there.

Stratospheric aerosol optical depth (AOD) is an indicator of volcanic eruptions that affect global climate and has been estimated from various information (e.g., Sato et al., 1993; Robock, 2000; Vernier et al., 2011). Since 1960 astronomical observations such as solar and stellar extinction and lunar eclipses have become available from both hemispheres, and since 1979 extensive satellite measurements have begun with the Stratospheric Aerosol Monitor (SAM) II on the Nimbus-7 satellite. On the other hand, the global radiosonde network that provides global atmospheric (upper-air) temperature data has been operating since the 1940s, with improved spatial resolution since the late 1950s (Gaffen, 1994). Since 1979, again, extensive satellite temperature measurements have begun with the Microwave Sounding Unit (MSU) and Stratospheric Sounding Unit (SSU) instruments on the TIROS-N satellite and on the subsequent several National Oceanic and Atmospheric Administration (NOAA) satellites. Since 1998, the Advanced MSU-A (AMSU-A) instruments on several NOAA satellites have provided global temperature measurements. See, e.g., Cristy et al. (2003), Wang et al. (2012), Wang and Zou (2014), Zou et al. (2014), and Nash and Saunders (2015) for these satellite temperature measurements.

Since the late 1950s, there occurred three major volcanic eruptions that significantly affected global climate, which are Mount Agung (8° S, 116° E), Bali, Indonesia in March 1963, El Chichón (17° N, 93° W), Chiapas, Mexico in April 1982, and Mount Pinatubo (15° N, 120° E), Luzon, Philippines in June 1991. The volcanic explosivity index (VEI) of these eruptions are 6 for Mount Pinatubo, 5 for El Chichón, and 4 for Mount Agung (Robock, 2000). Free and Lanzante (2009) and Randel (2010) used homogenized radiosonde datasets while Santer et al. (2001) and Soden et al. (2002) used MSU

satellite data to investigate the tropospheric and stratospheric temperature response to these eruptions. When extracting the volcanic signals, one needs a good evaluation, at the same time, of the components of El Niño Southern Oscillation (ENSO), Quasi-Biennial Oscillation (QBO), and 11 year solar cycle as well as seasonal variations and

5 linear trends. Each of the above four studies used a variety of regression analyses.

An atmospheric reanalysis dataset is constructed as a best estimate of the past state of the atmosphere using atmospheric observations with a fixed assimilation scheme and a fixed global forecast model (Trenberth and Olson, 1988; Bengtsson and Shukla, 1988). Using a fixed assimilation-forecast model prevents artificial changes being pro-

10 duced in the analysed fields due to system changes, but as described above, the observational data inputs still vary over the period of the reanalysis. Currently, there are about 10 global atmospheric reanalysis datasets available worldwide. Table 1 lists the reanalysis datasets considered in this study. It is known that different reanalysis datasets give different results for the same diagnostic. Depending on the diagnostic,

15 the different results may be due to differences either in the observational data assimilated, the assimilation scheme or forecast model, or any combination of these (see, e.g., Fujiwara et al., 2012 for a list of some examples). It is therefore necessary to compare all (or some of the newer) reanalysis datasets for various key diagnostics for understanding of the data quality and for future reanalysis improvements (Fujiwara and

20 Jackson, 2013).

Recently, Mitchell et al. (2015) analysed temperature and zonal wind data from nine reanalysis datasets using a linear multiple regression technique during the period from 1979 to 2009 by considering QBO, ENSO, AOD as a volcanic index, and solar cycle, with a focus on the solar cycle response. However, the volcanic response shown by

25 Mitchell et al. is a combined response due to the major eruptions over the period 1979–2009 (i.e., El Chichón in 1982 and Mount Pinatubo in 1991).

Investigation of climatic response to individual volcanic eruptions using reanalysis datasets is rather limited. For example, Harris and Highwood (2011) showed global mean surface temperature changes following the Pinatubo eruption using NCEP-1 and

ing volcanic signals. Such an analysis would also be valuable when assessing one of the proposed geoengineering options, i.e., stratospheric aerosol injection to counteract global surface warming (e.g., Crutzen, 2006; Robock et al., 2013).

In the present study, we analyse zonal and monthly mean temperature data from nine reanalysis datasets to investigate the response to the Mount Agung, El Chichón and Mount Pinatubo eruptions separately. Three other smaller-scale eruptions, Mount Awu (4° N, 125° E), Indonesia in August 1966 (VEI 4, Sato et al., 1993), Fernandina Island (0° S, 92° W) in the Galápagos Islands in June 1968 (VEI 4, Sato et al., 1993), and Mount Fuego (14° N, 91° W), Guatemala, in October–December 1974 (VEI 4, Smithsonian Institution National Museum of Natural History Global Volcanism Program, http://www.volcano.si.edu/, last accessed March 2015), are also analysed using the same method. The temperature response to the Mount Agung eruption and other three eruptions during the 1960s and 1970s is investigated using four reanalysis datasets (JRA-55, ERA-40, NCEP-1, and 20CR) that cover the period back to the 1960s. A multiple regression technique is used to remove the effects of seasonal variations, linear trends, QBO, solar cycle, and ENSO, and the residual time series is assumed to be composed of volcanic effects and random variations. The remainder of this paper is organized as follows. Section 2 describes the datasets and analysis method. Section 3 provides results and discussion. Finally, Sect. 4 lists the main conclusions.

2   Data and method

Monthly mean pressure-level temperature data from the nine reanalysis datasets listed in Table 1 were downloaded from each reanalysis-centre website or the US National

Center for Atmospheric Research (NCAR) Research Data Archive (http://rda.ucar.edu/). Zonal means were derived for each dataset before the analysis. All the reanalysis datasets except 20CR assimilated upper-air temperature measurements from radiosondes and from SSU, MSU, and AMSU-A satellite instruments, with varied assimilation techniques. 20CR assimilated only surface pressure reports and used observed monthly sea-surface temperature and sea-ice distributions as boundary conditions for the forecast model. Note also that for the 20CR, annual averages of volcanic aerosols were specified in the forecast model. Therefore, 20CR is expected to show volcanic signals even though it did not assimilate upper-air temperature data. Among other reanalysis datasets, only NCEP-CFSR included stratospheric volcanic aerosols in the forecast model. See Mitchell et al. (2015) for further technical comparisons among different reanalysis datasets. For a complete description of each reanalysis, see the reference papers shown in Table 1.

Table 1 also shows the period of data availability for each reanalysis dataset. For a direct intercomparison, we define two analysis periods, namely, between 1979 and 2009 (31 years) for eight reanalysis datasets (all except ERA-40) and between 1958 and 2001 (44 years) for four reanalysis datasets (JRA-55, ERA-40, NCEP-1, and 20CR). The former covers the eruptions of El Chichón in 1982 and Mount Pinatubo in 1991, while the latter also covers the eruption of Mount Agung in 1963 and three other smaller-scale eruptions during the 1960s and 1970s. Results from JRA-55, NCEP-1, and 20CR for the El Chichón and Mount Pinatubo eruptions for the two different-period analyses also provide an opportunity to investigate sensitivity to the choice of analysis period.

A multiple regression technique is applied to extract volcanic signals (e.g., Randel and Cobb, 1994; Randel, 2010; von Storch and Zwiers, 1999, Chapt. 8.4). First, all major variabilities, except for volcanic effects, were evaluated and subtracted from the original zonal and monthly mean temperature data. The major variabilities include seasonal harmonics of the form, $a_1 \sin \omega t + a_2 \cos \omega t + a_3 \sin 2\omega t + a_4 \cos 2\omega t + a_5 \sin 3\omega t + a_6 \cos 3\omega t$, with $\omega = 2\pi/(12\,\mathrm{mon})$, linear trends, two QBO indices, ENSO, and solar cy-

cle. For the latter five climatic indices, the six seasonal harmonics and a constant are further considered to construct seven indices for each of the five indices, as was done by Randel and Cobb (1994). For the two QBO indices, we use 20 and 50 hPa monthly mean zonal wind data taken at equatorial radiosonde stations provided by the Freie Universität Berlin. The cross-correlation coefficient for these two QBO indices is −0.24 for 1979–2009 and −0.21 for 1958–2001. For the ENSO index, we use the Niño 3.4 index, which is a standardized sea surface temperature anomaly in the Niño 3.4 region (5° N–5° S, 170–120° W), provided by the NOAA Climate Prediction Center. As is often done, a time lag for atmospheric response is considered for the ENSO index. We chose 4 months for the lag, following Free and Lanzante (2009). We confirmed that changing the ENSO lag from 0 to 6 months gives somewhat different ENSO signals particularly in the tropical stratosphere but does not alter other signals, including volcanic signals, significantly. For the solar cycle index, we use solar 10.7 cm flux data provided by the NOAA Earth System Research Laboratory. The multiple regression model that we use in this study is therefore,

$$Y(t) = a_0 + \sum_{l=1}^{41} a_l x_l(t) + R(t), \tag{1}$$

where $Y(t)$ is the zonal and monthly mean temperature time series at a particular latitude and pressure grid point, and a_l is the least squares solution of a parameter for climatic index time series $x_l(t)$. $R(t)$ is the residual of this model which is assumed to be composed of volcanic signals and random variations (Randel, 2010). Then, by following Randel (2010), the volcanic signal for each eruption is defined as the difference between the 12 month averaged $R(t)$ after each eruption and the 36 month averaged $R(t)$ before each eruption. There are several other possible minor variations for the methodological details, i.e., for the multiple regression model, the choice of particular index datasets, and the volcanic signal definition. The use of a consistent methodology is important for comparisons of different datasets. Where possible, however, we will discuss the methodological dependence below.

3   Results and discussion

3.1   The 1979–2009 analysis

Figures 1 and 2 show temperature variations in association with QBO, solar cycle and ENSO from JRA-55 and MERRA, respectively, for the region from 1000 to 1 hPa. The coloured regions are those evaluated as statistically significant at the 95 % confidence level (von Storch and Zwiers, 1999, Chapt. 8.4.6), with an effective degree of freedom where data are assumed to be independent for every three months. Comparing with the results from Mitchell et al. (2015) who used a regression analysis with different details, the setting of this effective degree of freedom may be somewhat too conservative. The general features are quite similar to those shown in Mitchell et al. (2015) although they also considered a volcanic index in the multiple regression analysis. The two QBO variations are displaced vertically in a quarter cycle in the tropics because of their downward phase propagation. The temperature QBO has off-equatorial out-of-phase signals centred around 30° N and around 30° S because of the associated secondary meridional circulation (Baldwin et al., 2001). The major features of the solar cycle variations are the tropical lower stratospheric warming. The ENSO features include the tropical tropospheric warming and a hint of tropical stratospheric cooling, although the statistical significance of this latter signal is weak. The strength of this cooling signal is sensitive to the choice of the time lag for the ENSO index (4 months in this study and 0 month in Mitchell et al., 2015). There also exists midlatitude lower stratospheric warming in both hemispheres for ENSO. The signals of QBO, solar cycle, and ENSO in the other 6 reanalysis datasets (ERA-Interim, NCEP-CFSR, JRA-25, NCEP-1, NCEP-2, and 20CR; not shown) are also similar to those in Mitchell et al. (2015). 20CR shows no QBO signals and no tropical stratospheric solar response. NCEP-CFSR shows weaker tropical lower stratospheric solar cycle warming. The overall agreement with the results in Mitchell et al. (2015) supports the assumption that the residual $R(t)$ is composed of volcanic signals and random variations.

Figure 3 shows the residual time series averaged for 30° N–30° S at 50 and at 300 hPa together with the lower-to-middle stratospheric AOD time series averaged for 27.4° N–27.4° S provided by the NASA Goddard Institute for Space Studies (Sato et al., 1993). The AOD time series clearly shows the timing of the El Chichón eruption and Mount Pinatubo eruption and the duration of their impact on the stratospheric aerosol loading. At 50 hPa, all reanalysis datasets show 1–2 K peak warming within one year after the El Chichón eruption, and most (except 20CR and JRA-25) show 2–2.5 K peak warming within one year after the Mount Pinatubo eruption. As described in Sect. 2, 20CR does not assimilate upper-air data, but incorporates annual averages of volcanic aerosols in the forecast model. Thus, 20CR shows a warming signal in association with both eruptions, though the one for Mount Pinatubo is smaller and slower. 20CR also shows warming signals in 1989 and in 1990 though all other datasets do not show the corresponding signals. The warming in JRA-25 is ∼ 1 K smaller than other reanalysis datasets except 20CR. This cold bias can be seen at least during the period 1988–1994. This may be in part due to the known stratospheric cold bias in JRA-25 (Onogi et al., 2007). The radiative scheme used in the JRA-25 forecast model has a known cold bias in the stratosphere, and the TOVS SSU/MSU measurements do not have enough number of channels to correct the model's cold bias; after introducing the ATOVS AMSU-A measurements in 1998, such a cold bias disappeared in the JRA-25 data product. As described in Sect. 2, NCEP-CFSR is the only reanalysis (except 20CR) that included stratospheric volcanic aerosols in the forecast model, but no clear difference is found in comparison with other recent reanalysis datasets. At 300 hPa, all reanalysis datasets show 0.4–0.8 K peak cooling within one year after the Mount Pinatubo eruption. No clear signals are found at 300 hPa for the El Chichón eruption. Note that the SD of the residual time series is ∼ 1 K for tropical 50 hPa and ∼ 0.3 K for tropical 300 hPa for all the datasets; thus, the volcanic signals discussed above are distinguishable from random variations.

Figure 4 shows the temperature signals for the El Chichón eruption from the 8 reanalysis datasets. As described in Sect. 2, the volcanic signal is defined as the difference

between the 12 month averaged $R(t)$ after each eruption and the 36 month averaged $R(t)$ before each eruption. The coloured regions are also defined by following Randel (2010), i.e., as those regions with positive (negative) values more (less) than twice the SD of annual mean residual $\overline{R(t)}$. The annual mean is taken here because of the use of 12 month average in the volcanic signal definition. For the most recent four reanalysis datasets, i.e., JRA-55, MERRA, ERA-Interim, and NCEP-CFSR, the tropical lower stratospheric warming of 1.2–1.6 K centred around 50–30 hPa is a common signal. There are also Northern Hemisphere midlatitude lower stratospheric warming and tropical upper stratospheric cooling signals, though the latter is comparable to random variations in some of the four datasets and thus its statistical significance is weak. The tropical and midlatitude troposphere is only weakly cooling, with a maximum cooling (0.4–0.8 K) occurring in the upper troposphere at 20–30° N. For JRA-25, the tropical lower stratospheric warming is confined around 100–50 hPa with (statistically insignificant) cooling signals around 50–10 hPa. This may be due to the cold bias in JRA-25 as described in the previous paragraph. The tropospheric features in JRA-25 are similar to those in the latest four reanalysis datasets. For NCEP-1 and NCEP-2, the tropical stratospheric warming region extends to 10 hPa where it maximises, and the 20–30° N upper tropospheric cooling is largely missing. For 20CR, tropical stratospheric warming is present, but this is due to the specified volcanic aerosols in the forecast model.

Free and Lanzante (2009) and Randel (2010) analysed the temperature signals for the El Chichón eruption using different homogenized radiosonde datasets globally up to the 30 hPa level. The distribution of the tropical lower stratospheric warming signal is similar, though the peak warming is greater, i.e., 1.6–2 K for Free and Lanzante (2009) and 2.5–3 K for Randel (2010). (Note that Free and Lanzante defined the volcanic signals as the difference between the 24 month average after the eruption and the 24 month average before the eruption.) Free and Lanzante (2009) also show a 20–30° N upper tropospheric cooling of 0.6–0.9 K.

Figure 5 shows the temperature signals for the Mount Pinatubo eruption. For the latest four reanalysis datasets, i.e., JRA-55, MERRA, ERA-Interim, and NCEP-CFSR,

the tropical lower stratospheric warming of 2.0–2.8 K (depending on datasets) centred around 50–30 hPa is a common signal. In the upper troposphere, a cooling (0.4–0.8 K) at 20–30° N and at 15–45° S can be seen, with the latter somewhat greater. JRA-25 shows similar upper tropospheric features and relatively similar lower stratospheric features, though for the latter, the warming magnitude is smaller and the "random" variability becomes large above the 50 hPa level because of the reason described above. For NCEP-1 and NCEP-2, the tropical tropospheric and stratospheric features are similar to those for the latest four reanalysis datasets, though the lower stratospheric warming magnitude is somewhat small. For 20CR, the tropical stratospheric warming is not detected. This is because of the unknown warming signals in 20CR in 1989 and in 1990 (see Fig. 3) that raised the 36 month averaged base in the volcanic signal definition.

The temperature signals for the Mount Pinatubo eruption shown in Randel (2010) are similar to the present results both in the tropical-midlatitude stratosphere and troposphere, though Randel's stratospheric warming peak value is somewhat greater (~ 3 K) and his upper tropospheric cooling is somewhat greater (0.5–1 K) and more uniform in latitude. On the other hand, Free and Lanzante (2009) show that the lower stratospheric warming signal is split near the equator with two maxima (1.6–2 K at 10° N and > 2 K at 15° S, both at 70–50 hPa) and that the upper tropospheric cooling signal has its peak (0.9–1.2 K) around 20° S. In summary, the latest four reanalysis datasets give more consistent signals for both eruptions compared to the two radiosonde data analyses using different homogenized datasets by Free and Lanzante (2009) and Randel (2010).

3.2 The 1958–2001 analysis

The multiple regression analysis is applied to the four reanalysis datasets, namely, JRA-55, ERA-40, NCEP-1, and 20CR which cover the period of 1958–2001. Figure 6 shows temperature variations associated with the QBO, solar cycle, and ENSO from JRA-55. Comparing with the 1979–2009 analysis results shown in Fig. 1, all variations are quite similar, with the statistically significant regions for the solar cycle variation

being much greater both in the tropical stratosphere and in the tropical troposphere. The same is true for NCEP-1 (not shown). 20CR does not have QBO and stratospheric solar-cycle signals, but does show ENSO signals in both 1979–2009 and 1958–2001 analyses; the 20CR ENSO signals are similar to those from all other reanalysis datasets. ERA-40 shows similar results to JRA-55 except for the solar cycle variation. In ERA-40, the tropical lower stratospheric warming signal in association with the solar cycle is very weak and not symmetric about the equator, in contrast to the results by Crooks and Gray (2005) and Mitchell et al. (2015) who both applied a regression analysis during the period 1979–2001.

Figure 7 shows the time series of residual $R(t)$ and stratospheric AOD averaged over the tropics for the period between 1958 and 2001. The AOD time series shows the timing of the Mount Agung eruption in March 1963 as well as the El Chichón and Mount Pinatubo eruptions. The features at both 50 and 300 hPa for the El Chichón and Mount Pinatubo eruptions are quite similar to the 1979–2009 analysis results shown in Fig. 3, including the 20CR's smaller and slower Mount Pinatubo signal at 50 hPa. For the Mount Agung eruption, ∼ 2.5 K peak warming is seen within one year after the eruption except for 20CR. At 300 hPa, a sudden cooling occurred in mid-1964 for all the datasets, which is probably related to the Mount Agung eruption. ERA-40 shows anomalous ∼ 1 K warming in the mid-1970s at both levels, which are not present in other reanalysis datasets (see also Fig. 14 of Kobayashi et al., 2015).

Figure 8 shows the temperature signals for the Mount Agung eruption from 4 different reanalysis datasets. All except 20CR show Southern Hemisphere lower stratospheric warming centred at 40–30° S and 100–50 hPa, with an extension to equatorial latitudes at 50 hPa. The maximum warming value varies with dataset, that is, 1.6–2 K for NCEP-1, 2–2.4 K for JRA-55, and 2.4–2.8 K for ERA-40. The reason for the weak signal in 20CR is in the fact that 20CR does not assimilate upper-air temperature observations but does consider volcanic aerosol loading in the forecast model. The modelled aerosol loading was probably too weak. The 300 hPa cooling shown in Fig. 7 is not

captured with the current volcanic-signal definition (i.e., 12 month average after the eruption started).

Free and Lanzante (2009) showed a very similar Southern Hemisphere midlatitude lower stratospheric warming signal ($> 2\,\mathrm{K}$) in association with the Mount Agung eruption using a homogenized radiosonde dataset. Sato et al. (1993) showed that the aerosols emitted from the Mount Agung eruption were transported primarily to the Southern Hemisphere. Figure 9 shows time-latitude distributions of temperature residual at 50 hPa and at 300 hPa from JRA-55 and of the stratospheric AOD. The aerosol loading due to the El Chichón and Mount Pinatubo eruptions was very large in the tropics and extended to both hemispheres, while that due to the Mount Agung eruption extended primarily to the Southern Hemisphere.

The El Chichón signal from the 1958–2001 analysis (not shown) is very similar to the one from the 1979–2009 analysis for JRA-55 and 20CR shown in Fig. 4. For NCEP-1, the warming signal in the tropical 30–10 hPa shown in Fig. 4 becomes weaker, thus showing better agreement with the results from the modern reanalysis datasets (e.g., JRA-55). ERA-40 shows similar signal to JRA-55 at least up to the 10 hPa level globally. The Mount Pinatubo signal from the 1958–2001 analysis (not shown) is very similar to the one from the 1979–2009 analysis for JRA-55, NCEP-1, and 20CR. ERA-40 shows similar signal to JRA-55 at least up to the 20 hPa level globally.

The AOD time series in Figs. 7 and 9 also shows two smaller aerosol loading cases, i.e., in 1968/69 and in 1975. The former may correspond to the eruption of Fernandina Island in the Galápagos Islands, Ecuador in June 1968 (Sato et al., 1993). The latter may correspond to the eruption of Mount Fuego, Guatemala, in October–December 1974 (Smithsonian Institution National Museum of Natural History Global Volcanism Program, http://www.volcano.si.edu/, last accessed March 2015). The same volcanic-signal definition, i.e., the difference between the 12 month averaged $R(t)$ after each eruption and the 36 month averaged $R(t)$ before each eruption, was applied. Interestingly, for the Fernandina Island case (Fig. 10), JRA-55 and NCEP-1 show tropical upper tropospheric warming (peak value of 0.4–0.8 K at 300 hPa) and tropical

100–50 hPa cooling (1.2–1.6 K for JRA-55 and 1.6–2.0 K for NCEP-1), which is opposite to the response following the 3 major eruptions previously examined. ERA-40 shows a similar tropical lower stratospheric cooling, and ERA-40 and 20CR shows much weaker tropical tropospheric warming. It is possible that the upper tropospheric warming signal is a radiative response to aerosols that did not penetrate so deeply into the stratosphere. In addition, despite the inclusion of QBO indices in the regression analysis, the residual signal (interpreted as the volcanic response) has a structure in the stratosphere similar to the QBO response, with a tropical signal whose sign alternates in the vertical direction plus a weaker subtropical response of opposite sign. For the Mount Fuego case (not shown), ERA-40 showed very different signals from other three reanalysis datasets, as can be inferred from Fig. 7, and all four datasets basically showed no substantial signal exceeding twice the SD of annual mean residual. There also occurred an eruption of Mount Awu, Indonesia in August 1966 (Sato et al., 1993), but the AOD time series do not show any substantial signal (Fig. 7). The same volcanic analysis for Mount Awu eruption showed cooling (0.8–1.6 K) in the Southern Hemisphere midlatitude lower stratosphere for all the four datasets (not shown).

Figure 9 provides a useful summary plot for the volcanic effects on the temperature using JRA-55 from the 1958–2001 analysis together with the AOD latitudinal time series. The tropical lower stratosphere warmed after the three major volcanic eruptions, Mount Agung in March 1963, El Chichón in April 1982, and Mount Pinatubo in June 1991 with a time scale of 1–2 years. The warming after the Mount Agung eruption is not equatorially symmetric and is shifted to the Southern Hemisphere and to somewhat lower levels, in association with the distribution of aerosol loading. The tropical troposphere became cooler after the Mount Pinatubo eruption but the tropospheric response is not clear for the other two eruptions. The high latitude response is also unclear both in the troposphere and stratosphere due to high random variations that mask any volcanic signals, if they exist. The smaller-scale Fernandina Island eruption in June 1968 may have had weak but opposite effects, i.e., tropical lower stratospheric cooling and tropical upper tropospheric warming.

4   Conclusions

Monthly and zonal mean temperature data from nine reanalysis datasets were analysed to characterize the response to the three major volcanic eruptions and three other smaller-scale eruptions during the 1960s to 1990s. Multiple linear regression analysis was applied to evaluate seasonal variations, trends, QBO, solar cycle and ENSO components, and the residual time series $R(t)$ was assumed to be composed of volcanic signals and random variations. The volcanic signals were defined as the difference between the 12 month averaged $R(t)$ after each eruption and the 36 month averaged $R(t)$ before each eruption. Two separate analyses were performed, that is, one for the period 1979–2009 (31 years) using eight reanalysis datasets and the other for 1958–2001 (44 years) using four reanalysis datasets. The former covered the eruptions of El Chichón (April 1982) and Mount Pinatubo (June 1991), while the latter also covered those of Mount Agung (March 1963), Mount Awu (August 1966), Fernandina Island (June 1968) and Mount Fuego (October–December 1974).

The general features of the response to QBO, solar cycle, and ENSO were found to be quite similar to those shown in Mitchell et al. (2015) who also used a multiple linear regression with different methodological details, in particular, considering a volcanic index as well. Also, these signals were at least qualitatively similar among reanalysis datasets, with a notable exception that 20CR shows no QBO signals and no tropical stratospheric solar response.

The latitude-pressure distribution of El Chichón and Mount Pinatubo temperature response was quite similar at least among the four latest reanalysis datasets (JRA-55, MERRA, ERA-Interim, and NCEP-CFSR) and between the 1979–2009 and 1958–2001 analyses. For the Mount Pinatubo eruption, tropical lower stratospheric warming and tropical upper tropospheric cooling were observed. For the El Chichón eruption, tropical lower stratospheric warming was observed, but tropospheric cooling was much weaker than the Mount Pinatubo case. For the Mount Agung eruption, JRA-55, ERA-40, and NCEP-1 showed Southern Hemisphere lower stratospheric warming centred

Response to volcanic eruptions in reanalyses

M. Fujiwara et al.

Back   Close

Full Screen / Esc

Printer-friendly Version

Interactive Discussion

at 40–30° S and 100–50 hPa, with an equatorial extension to 50 hPa. Thus, the Agung signal was asymmetric about the equator and very different from the El Chichón and Pinatubo signals. We suggest that this may be due to differences in the transport of volcanic aerosols (Sato et al., 1993). There were some other smaller-scale tropical eruptions during the 1960s and 1970s. Among them, the Fernandina Island case showed tropical upper tropospheric weak warming and tropical lower stratospheric cooling, i.e., with opposite signs to the three major eruptions. The Awu also showed Southern Hemisphere midlatitude lower stratospheric cooling.

It was found that the temperature response was different for different eruptions even for the three major eruptions. In particular, wide-spread upper tropospheric cooling was observed only for the Mount Pinatubo case. The Mount Agung lower stratospheric response was found to be asymmetric about the equator. Smaller-scale eruptions may have resulted in very different climatic response, such as lower stratospheric cooling, not warming, although the cases are limited. The characteristics in the temperature response are related to the transport of stratospheric aerosols together with the amount of sulphur species emitted into the stratosphere. Depending on the location, season, and magnitude of the eruption, the climatic response can be very different (e.g., Trepte and Hitchman, 1992). This needs to be taken into account when evaluating the stratospheric sulphur injection as a geo-engineering option, and thus accurate estimations of stratospheric circulation and transport are essential for assessing the climate impacts. Also, it should be noted that accurate evaluation of naturally induced variability such as QBO, solar cycle, and ENSO is necessary to detect the effects of artificial injection. Finally, reanalysis intercomparison for this case gave us some more confidence on the volcanic and other naturally induced effects, even if there are several known issues (e.g., inhomogeneity of observational data) in the current reanalysis systems.

Title Page

Abstract | Introduction

Conclusions | References

Tables | Figures

|◀ | ▶|

◀ | ▶

Back | Close

Full Screen / Esc

Printer-friendly Version

Interactive Discussion

References

Baldwin, M. P., Gray, L. J., Dunkerton, T. J., Hamilton, K., Haynes, P. H., Randel, W. J., Holton, J. R., Alexander, M. J., Hirota, I., Horinouchi, T., Jones, D. B. A., Kinnersley, J. S., Marquardt, C., Sato, K., and Takahashi, M.: The quasi-biennial oscillation, Rev. Geophys., 39, 179–229, doi:10.1029/1999RG000073, 2001.

Bengtsson, L. and Shukla, J.: Integration of space and in situ observations to study global climate change, B. Am. Meteorol. Soc., 69, 1130–1143, 1988.

Butchart, N.: The Brewer–Dobson Circulation, Rev. Geophys., 52, 157–184, doi:10.1002/2013RG000448, 2014.

Christy, J. R., Spencer, R. W., Norris, W. B., and Braswell, W. D.: Error estimates of version 5.0 of MSU-AMSU bulk atmospheric temperature, J. Atmos. Ocean. Tech., 20, 613–629, 2003.

Compo, G. P., Whitaker, J. S., Sardeshmukh, P. D., Matsui, N., Allan, R. J., Yin, X., Gleason, B. E., Vose, R. S., Rutledge, G., Bessemoulin, P., Brönnimann, S., Brunet, M., Crouthamel, R. I., Grant, A. N., Groisman, P. Y., Jones, P. D., Kruk, M. C., Kruger, A. C., Marshall, G. J., Maugeri, M., Mok, H. Y., Nordli, Ø., Ross, T. F., Trigo, R. M., Wang, X. L., Woodruff, S. D., and Worley, S. J.: The twentieth century reanalysis project, Q. J. Roy. Meteor. Soc., 137, 1–28, doi:10.1002/qj.776, 2011.

Crooks, S. A. and Gray, L. J.: Characterization of the 11-year solar signal using a multiple regression analysis of the ERA-40 dataset, J. Climate, 18, 996–1015, 2005.

Crutzen, P. J.: Albedo enhancement by stratospheric sulfur injections: a contribution to resolve a policy dilemma?, Climatic Change, 77, 211–220, doi:10.1007/s10584-006-9101-y, 2006.

Dee, D. P., Uppala, S. M., Simmons, A. J., Berrisford, P., Poli, P., Kobayashi, S., Andrae, U., Balmaseda, M. A., Balsamo, G., Bauer, P., Bechtold, P., Beljaars, A. C. M., van de Berg, L., Bidlot, J., Bormann, N., Delsol, C., Dragani, R., Fuentes, M., Geer, A. J., Haimberger, L., Healy, S. B., Hersbach, H., Hólm, E. V., Isaksen, L., Kållberg, P., Köhler, M., Matricardi, M., McNally, A. P., Monge-Sanz, B. M., Morcrette, J.-J., Park, B.-K., Peubey, C., de Rosnay, P., Tavolato, C., Thépaut, J.-N., and Vitart, F.: The ERA-Interim reanalysis: configuration and performance of the data assimilation system, Q. J. Roy. Meteor. Soc., 137, 553–597, doi:10.1002/qj.828, 2011.

Ebita, A., Kobayashi, S., Ota, Y., Moriya, M., Kumabe, R., Onogi, K., Harada, Y., Yasui, S., Miyaoka, K., Takahashi, K., Kamahori, H., Kobayashi, C., Endo, H., Soma, M., Oikawa, Y., and Ishimizu, T.: The Japanese 55-year reanalysis "JRA-55": an interim report, Sci. Online Lett. Atmos., 7, 149–152, doi:10.2151/sola.2011-038, 2011.

Free, M. and Lanzante, J.: Effect of volcanic eruptions on the vertical temperature profile in radiosonde data and climate models, J. Climate, 22, 2925–2939, doi:10.1175/2008JCLI2562.1, 2009.

Fujiwara, M. and Jackson, D.: SPARC Reanalysis Intercomparison Project (S-RIP) planning meeting, 29 April–1 May 2013, Exeter, UK, SPARC Newsletter, 41, 52–55, 2013.

Fujiwara, M., Polavarapu, S., and Jackson, D.: A proposal of the SPARC Reanalysis/Analysis Intercomparison Project, SPARC Newsletter, 38, 14–17, 2012.

Gaffen, D. J.: Temporal inhomogeneities in radiosonde temperature records, J. Geophys. Res., 99, 3667–3676, doi:10.1029/93JD03179, 1994.

Harris, B. M. and Highwood, E. J.: A simple relationship between volcanic sulfate aerosol optical depth and surface temperature change simulated in an atmosphere–ocean general circulation model, J. Geophys. Res., 116, D05109, doi:10.1029/2010JD014581, 2011.

Kalnay, E., Kanamitsu, M., Kistler, R., Collins, W., Deaven, D., Gandin, L., Iredell, M., Saha, S., White, G., Woollen, J., Zhu, Y., Leetmaa, A., Reynolds, R., Chelliah, M., Ebisuzaki, W., Higgins, W., Janowiak, J., Mo, K. C., Ropelewski, C., Wang, J., Jenne R., and Joseph, D.: The NCEP/NCAR 40-year reanalysis project, B. Am. Meteorol. Soc., 77, 437–471, 1996.

Kanamitsu, M., Ebisuzaki, W., Woollen, J., Yang, S.-K., Hnilo, J. J., Fiorino, M., and Potter, G. L.: NCEP–DOE AMIP-II reanalysis (R-2), B. Am. Meteorol. Soc., 83, 1631–1643, 2002.

Response to volcanic eruptions in reanalyses

M. Fujiwara et al.

Title Page

Abstract	Introduction
Conclusions	References
Tables	Figures

|◄ | ►|

◄ | ►

Back | Close

Full Screen / Esc

Printer-friendly Version

Interactive Discussion

Kistler, R., Collins, W., Saha, S., White, G., Woollen, J., Kalnay, E., Chelliah, M., Ebisuzaki, W., Kanamitsu, M., Kousky, V., van den Dool, H., Jenne, R., and Fiorino, M.: The NCEP–NCAR 50-year reanalysis: monthly means CD-ROM and documentation, B. Am. Meteorol. Soc., 82, 247–267, 2001.

Kobayashi, S., Ota, Y., Harada, Y., Ebita, A., Moriya, M., Onoda, H., Onogi, K., Kamahori, H., Kobayashi, C., Endo, H., Miyaoka, K., and Takahashi, K.: The JRA-55 reanalysis: general specifications and basic characteristics, J. Meteorol. Soc. Jpn., 93, 5–48, doi:10.2151/jmsj.2015-001, 2015.

Mitchell, D. M., Gray, L. J., Fujiwara, M., Hibino, T., Anstey, J. A., Ebisuzaki, W., Harada, Y., Long, C., Misios, S., Stott, P. A., and Tan, D.: Signatures of naturally induced variability in the atmosphere using multiple reanalysis datasets, Q. J. Roy. Meteor. Soc., accepted, doi:10.1002/qj.2492, 2015.

Nash, J. and Saunders, R.: A review of Stratospheric Sounding Unit radiance observations for climate trends and reanalyses, Q. J. Roy. Meteor. Soc., accepted, doi:10.1002/qj.2505, 2015.

Onogi, K., Tsutsui, J., Koide, H., Sakamoto, M., Kobayashi, S., Hatsushika, H., Matsumoto, T., Yamazaki, N., Kamahori, H., Takahashi, K., Kadokura, S., Wada, K., Kato, K., Oyama, R., Ose, T., Mannoji, N., and Taira, R.: The JRA-25 reanalysis, J. Meteorol. Soc. Jpn., 85, 369–432, doi:10.2151/jmsj.85.369, 2007.

Randel, W. J.: Variability and trends in stratospheric temperature and water vapor, in: The Stratosphere: Dynamics, Transport and Chemistry, Geophys. Monogr. Ser. 190, edited by: Polvani, L. M., Sobel, A. H., and Waugh, D. W., American Geophysical Union, Washington, D.C., USA, 123–135, 2010.

Randel, W. J. and Cobb, J. B.: Coherent variations of monthly mean total ozone and lower stratospheric temperature, J. Geophys. Res., 99, 5433–5447, 1994.

Rienecker, M. M., Suarez, M. J., Gelaro, R., Todling, R., Bacmeister, J., Liu, E., Bosilovich, M. G., Schubert, S. D., Takacs, L., Kim, G.-K., Bloom, S., Chen, J., Collins, D., Conaty, A., da Silva, A., Gu, W., Joiner, J., Koster, R. D., Lucchesi, R., Molod, A., Owens, T., Pawson, S., Pegion, P., Redder, C. R., Reichle, R., Robertson, F. R., Ruddick, A. G., Sienkiewicz, M., and Woollen, J.: MERRA: NASA's modern-era retrospective analysis for research and applications, J. Climate, 24, 3624–3648, doi:10.1175/JCLI-D-11-00015.1, 2011.

Robock, A.: Volcanic eruptions and climate, Rev. Geophys., 38, 191–219, doi:10.1029/1998RG000054, 2000.

Title Page

Abstract | Introduction

Conclusions | References

Tables | Figures

|◀ | ▶|

◀ | ▶

Back | Close

Full Screen / Esc

Printer-friendly Version

Interactive Discussion

Robock, A., MacMartin, D. G., Duren, R., and Christensen, M. W.: Studying geo-engineering with natural and anthropogenic analogs, Climatic Change, 121, 445–458, doi:10.1007/s10584-013-0777-5, 2013.

Saha, S., Moorthi, S., Pan, H.-L., Wu, X., Wang, J., Nadiga, S., Tripp, P., Kistler, R., Woollen, J., Behringer, D., Liu, H., Stokes, D., Grumbine, R., Gayno, G., Wang, J., Hou, Y.-T., Chuang, H.-Y., Juang, H.-M. H., Sela, J., Iredell, M., Treadon, R., Kleist, D., van Delst, P., Keyser, D., Derber, J., Ek, M., Meng, J., Wei, H., Yang, R., Lord, S., van den Dool, H., Kumar, A., Wang, W., Long, C., Chelliah, M., Xue, Y., Huang, B., Schemm, J.-K., Ebisuzaki, W., Lin, R., Xie, P., Chen, M., Zhou, S., Higgins, W., Zou, C.-Z., Liu, Q., Chen, Y., Han, Y., Cucurull, L., Reynolds, R. W., Rutledge, G., and Goldberg, M.: The NCEP climate forecast system reanalysis, B. Am. Meteorol. Soc., 91, 1015–1057, doi:10.1175/2010BAMS3001.1, 2010.

Santer, B. D., Wigley, T. M. L., Doutriaux, C., Boyle, J. S., Hansen, J. E., Jones, P. D., Meehl, G. A., Roeckner, E., Sengupta, S., and Taylor, K. E.: Accounting for the effects of volcanoes and ENSO in comparisons of modeled and observed temperature trends, J. Geophys. Res., 106, 28033–28059, doi:10.1029/2000JD000189, 2001.

Sato, M., Hansen, J. E., McCormick, M. P., and Pollack, J. B.: Stratospheric aerosol optical depths, 1850–1990, J. Geophys. Res., 98, 22987–22994, doi:10.1029/93JD02553, 1993.

Soden, B. J., Wetherald, R. T., Stenchikov, G. L., and Robock, A.: Global cooling after the eruption of Mount Pinatubo: a test of climate feedback by water vapor, Science, 296, 727–730, doi:10.1126/science.296.5568.727, 2002.

Trenberth, K. E. and Olson, J. G.: An evaluation and intercomparison of global analyses from the National Meteorological Center and the European Centre for Medium-Range Weather Forecasts, B. Am. Meteorol. Soc., 69, 1047–1057, 1988.

Trepte, C. R. and Hitchman, M. H.: Tropical stratospheric circulation deduced from satellite aerosol data, Nature, 355, 626–628, doi:10.1038/355626a0, 1992.

Uppala, S. M., Kållberg, P. W., Simmons, A. J., Andrae, U., Bechtold, V. D. C., Fiorino, M., Gibson, J. K., Haseler, J., Hernandez, A., Kelly, G. A., Li, X., Onogi, K., Saarinen, S., Sokka, N., Allan, R. P., Andersson, E., Arpe, K., Balmaseda, M. A., Beljaars, A. C. M., Berg, L. V. D., Bidlot, J., Bormann, N., Caires, S., Chevallier, F., Dethof, A., Dragosavac, M., Fisher, M., Fuentes, M., Hagemann, S., Hólm, E., Hoskins, B. J., Isaksen, L., Janssen, P. A. E. M., Jenne, R., Mcnally, A. P., Mahfouf, J.-F., Morcrette, J.-J., Rayner, N. A., Saunders, R. W., Simon, P., Sterl, A., Trenberth, K. E., Untch, A., Vasiljevic, D., Viterbo, P., and Woollen, J.:

The ERA-40 reanalysis, Q. J. Roy. Meteor. Soc., 131, 2961–3012, doi:10.1256/qj.04.176, 2005.

Vernier, J.-P., Thomason, L. W., Pommereau, J.-P., Bourassa, A., Pelon, J., Garnier, A., Hauchecorne, A., Blanot, L., Trepte, C., Degenstein, D., and Vargas, F.: Major influence of tropical volcanic eruptions on the stratospheric aerosol layer during the last decade, Geophys. Res. Lett., 38, L12807, doi:10.1029/2011GL047563, 2011.

von Storch, H. and Zwiers, F. W.: Statistical Analysis in Climatic Research, Cambridge Univ. Press, Cambridge, UK, 484 pp., 1999.

Wang, L., Zou, C.-Z., and Qian, H.: Construction of stratospheric temperature data records from Stratospheric Sounding Units, J. Climate, 25, 2931–2946, doi:10.1175/JCLI-D-11-00350.1, 2012.

Wang, W. and Zou, C.-Z.: AMSU-A-only atmospheric temperature data records from the lower troposphere to the top of the stratosphere, J. Atmos. Ocean. Tech., 31, 808–825, doi:10.1175/JTECH-D-13-00134.1, 2014.

Zou, C.-Z., Qian, H., Wang, W., Wang, L., and Long, C.: Recalibration and merging of SSU observations for stratospheric temperature trend studies, J. Geophys. Res., 119, 13180–13205, doi:10.1002/2014JD021603, 2014.

Table 1. List of global atmospheric reanalysis datasets considered in this study.

Dataset	Centre	Period	Reference
ERA-Interim	ECMWF	1979–present	Dee et al. (2011)
ERA-40	ECMWF	Sep 1957–Aug 2002	Uppala et al. (2005)
JRA-55	JMA	1958–present	Ebita et al. (2011); Kobayashi et al. (2015)
JRA-25/JCDAS	JMA and CRIEP	Jan 1979–Jan 2014	Onogi et al. (20 07)
MERRA	NASA	1979–present	Rienecker et al. (2011)
NCEP-CFSR	NOAA/NCEP	1979–2009, 2010[1]–present	Saha et al. (2010)
NCEP-DOE AMIP-II R-2 (NCEP-2)	NOAA/NCEP and DOE AMIP-II	1979–present	Kanamitsu et al. (2002)
NCEP-NCAR R-1 (NCEP-1)	NOAA/NCEP and NCAR	1948–present	Kalnay et al. (1996); Kistler et al. (2001)
NOAA-CIRES 20CR v2 (20CR)	NOAA and CIRES/Univ. Colorado	Nov 1869–Dec 2012	Compo et al. (2011)

[1] The model horizontal resolution has increased in 2010 in the NCEP-CFSR.

Response to volcanic eruptions in reanalyses

M. Fujiwara et al.

Title Page

Abstract | Introduction

Conclusions | References

Tables | Figures

|◀ | ▶|

◀ | ▶

Back | Close

Full Screen / Esc

Printer-friendly Version

Interactive Discussion

Figure 1. Latitude–pressure distribution of the temperature variations in association with (top left) QBO 20 hPa zonal wind index, (top right) QBO 50 hPa zonal wind index, (bottom left) solar cycle index, and (bottom right) ENSO index from JRA-55 reanalysis data for the period 1979–2009. The units are in Kelvin per SD of each index (note that each index time series was standardized before the regression analysis). Solid and dashed lines denote positive and negative values, respectively. The contour interval is 0.2 K for QBO, and 0.1 K for solar cycle and ENSO. Coloured regions denote those greater (orange) and smaller (blue) than random variations with the 95 % confidence interval at each location.

Title Page

Abstract | Introduction

Conclusions | References

Tables | Figures

◀ | ▶|

◀ | ▶

Back | Close

Full Screen / Esc

Printer-friendly Version

Interactive Discussion

Figure 2. As in Fig. 1 but for MERRA reanalysis data.

Full Screen / Esc

Printer-friendly Version

Interactive Discussion
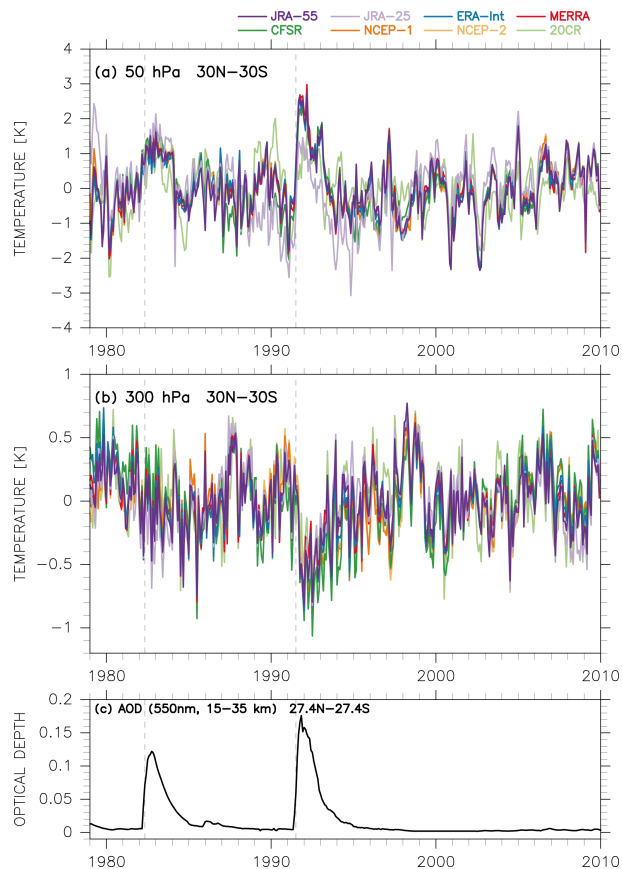
Figure 3. Time series of temperature residual $R(t)$ averaged for 30° N–30° S for the 1979–2009 regression analysis from eight reanalysis datasets at **(a)** 50 hPa and **(b)** 300 hPa. **(c)** Time series of aerosol optical depth at 550 nm averaged for 27.4° N–27.4° S and integrated for the region 15–35 km. Vertical dotted lines indicate the starting date of the two volcanic eruptions.
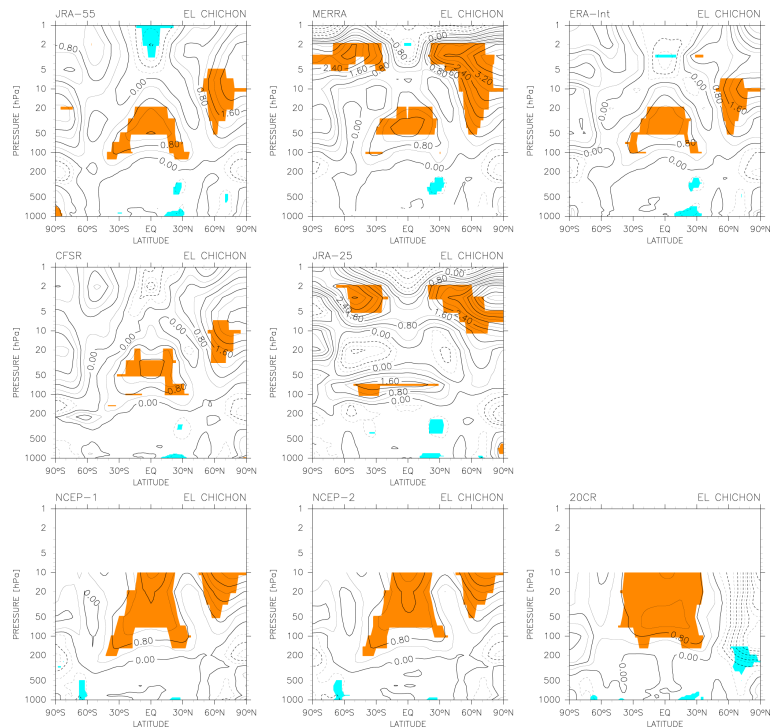
Figure 4. Latitude-pressure distribution of the temperature response to the El Chichón eruption in April 1982 for the 1979–2009 analysis from eight reanalysis datasets. Solid and dashed lines denote positive and negative values, respectively. The contour interval is 0.4 K. Coloured regions denote those with positive and greater (orange) and negative and smaller (blue) than twice the SD of annual mean residual $\overline{R(t)}$ at each location.
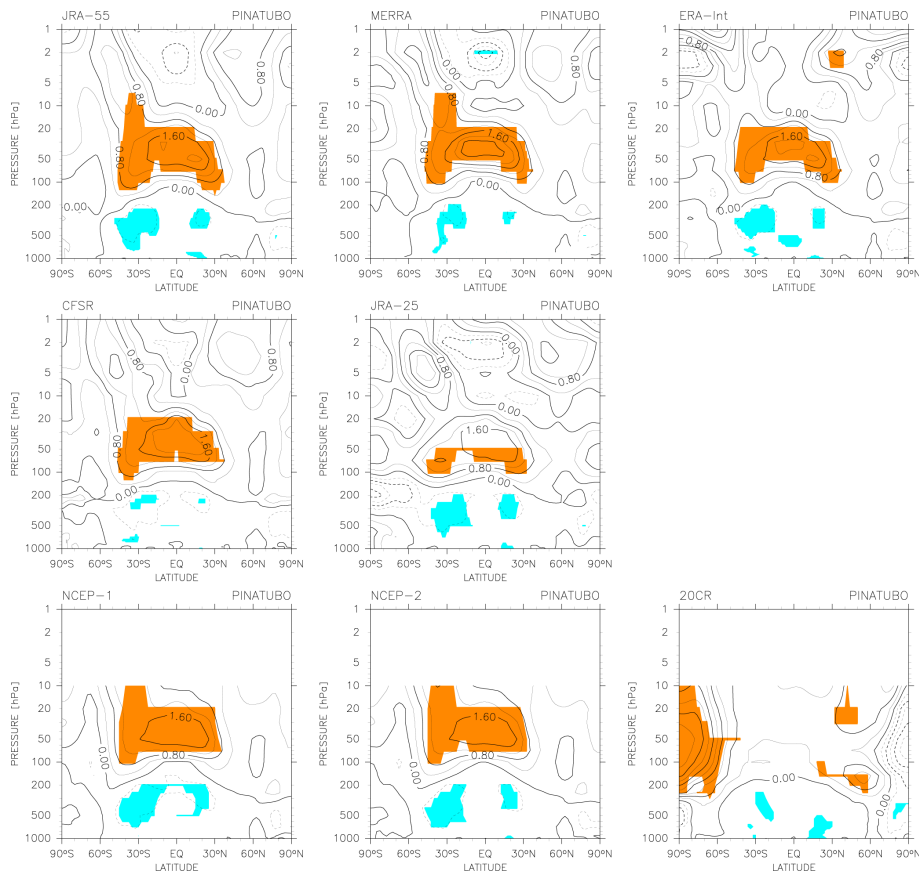
Figure 5. As in Fig. 4 but for the Mount Pinatubo eruption in June 1991.

Title Page

Abstract | Introduction

Conclusions | References

Tables | Figures

|◄ | ►|

◄ | ►

Back | Close

Full Screen / Esc

Printer-friendly Version

Interactive Discussion
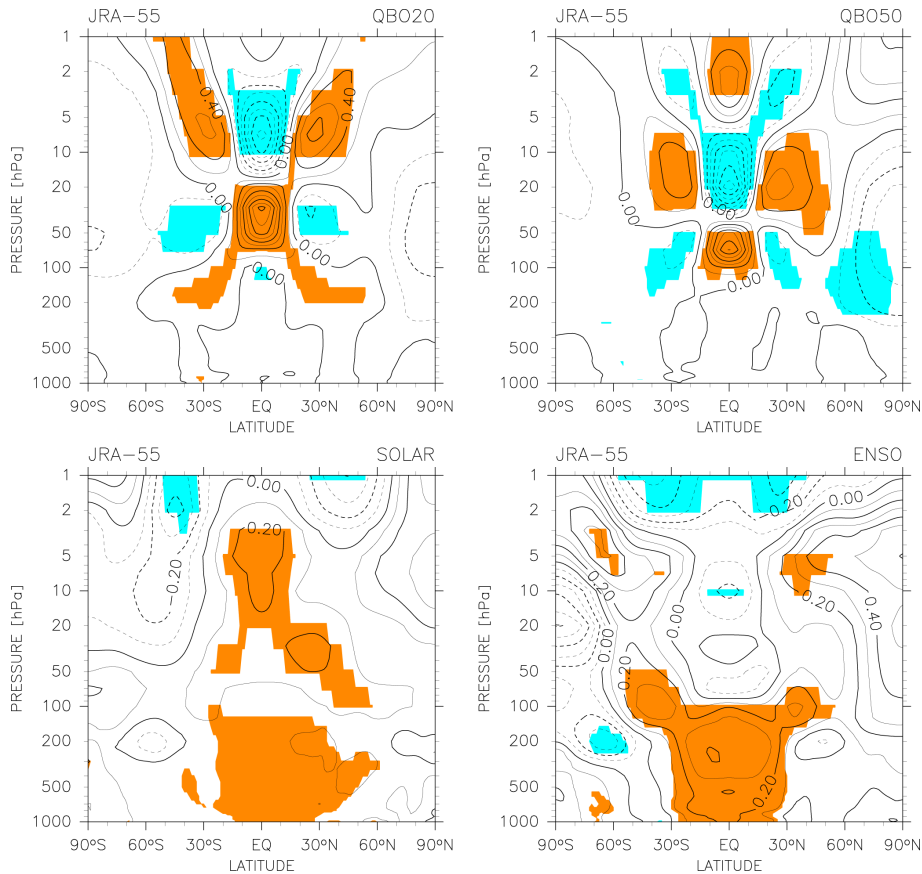
Figure 6. As in Fig. 1 but for the period 1958–2001.

Full Screen / Esc

Printer-friendly Version

Interactive Discussion
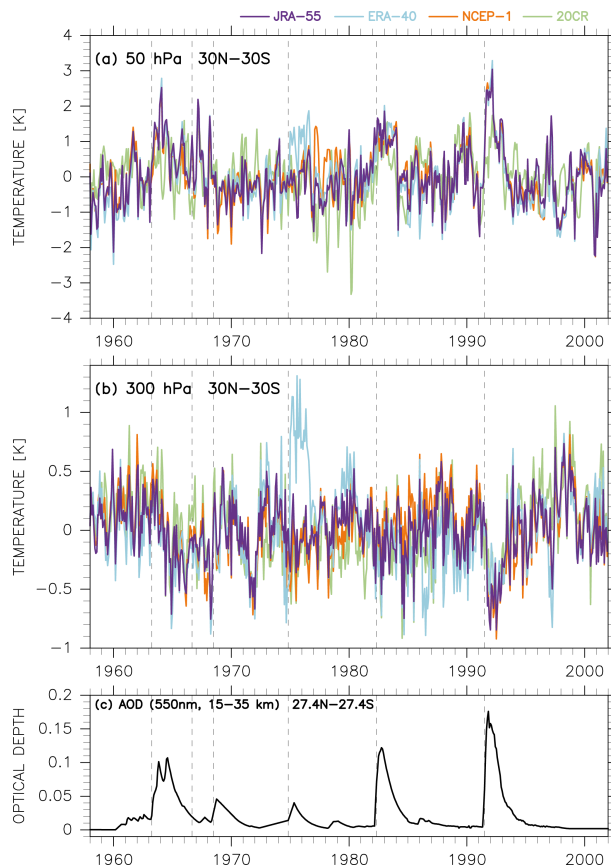
Figure 7. As in Fig. 3 but for the 1958–2001 regression analysis from four reanalysis datasets. Vertical dotted lines indicate the starting date of the six volcanic eruptions.
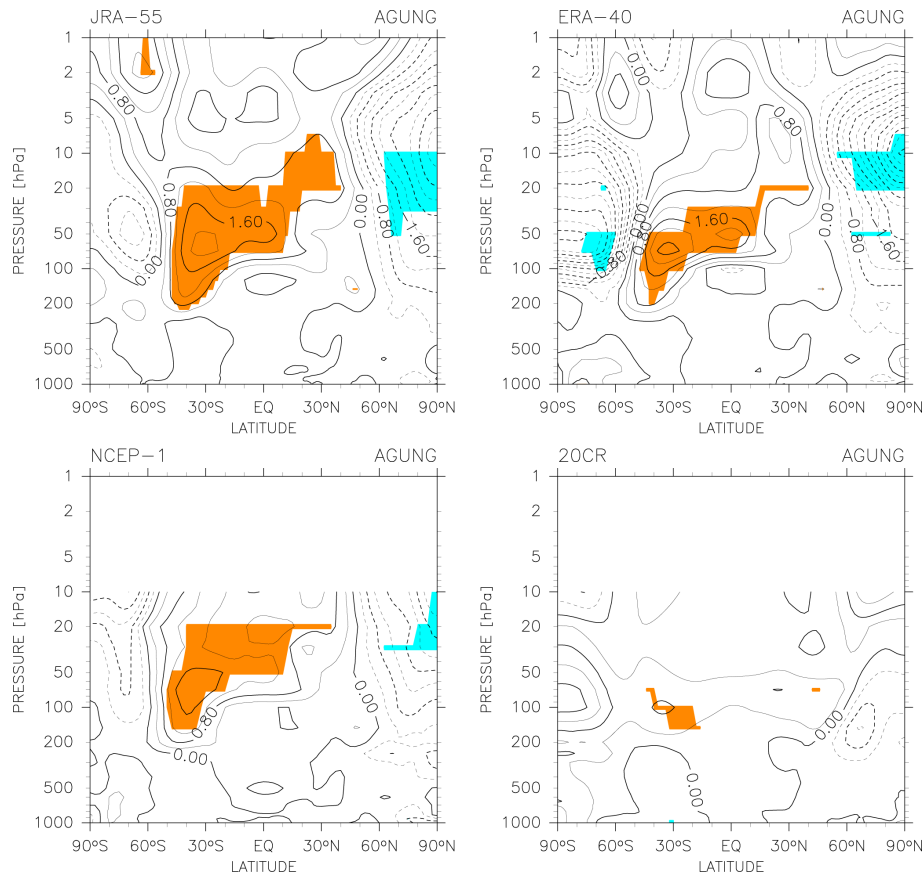
Figure 8. As in Fig. 4 but for the Mount Agung eruption in March 1963 for the 1958–2001 analysis from four reanalysis datasets.

Response to volcanic eruptions in reanalyses

M. Fujiwara et al.
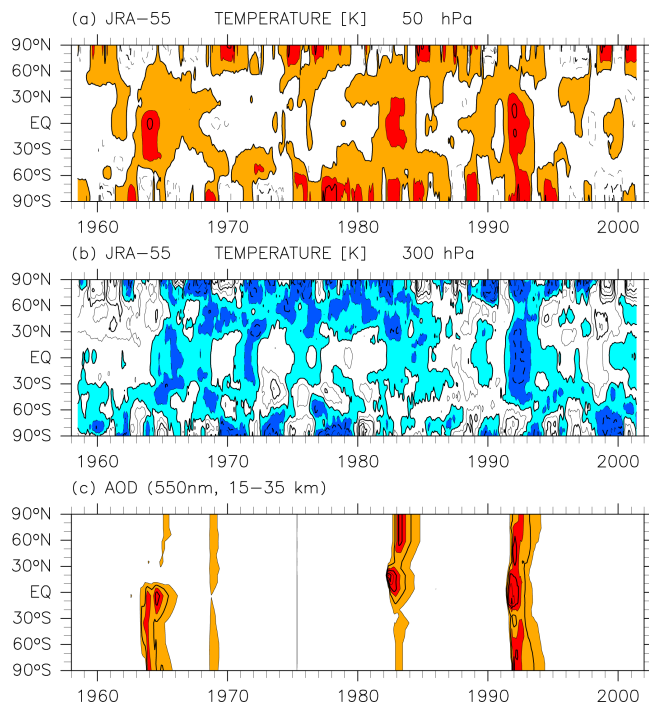
Figure 9. Time-latitude distribution of temperature residual $R(t)$ for the 1958–2001 regression analysis from JRA-55 reanalysis data at **(a)** 50 hPa and **(b)** 300 hPa. Thirteen-month running average has been taken for $R(t)$. The contour interval is 1.0 K for **(a)** and 0.25 K for **(b)**. The regions with 0–1 K (> 1 K) are coloured in orange (red) in **(a)**. The regions with 0 to -0.25 K (< -0.25 K) are coloured in light (dark) blue. **(c)** Time-latitude distribution of aerosol optical depth at 550 nm integrated for the region 15–35 km. The contour interval is 0.04. The regions with 0.04–0.12 (> 0.12) are coloured in orange (red) in **(c)**.
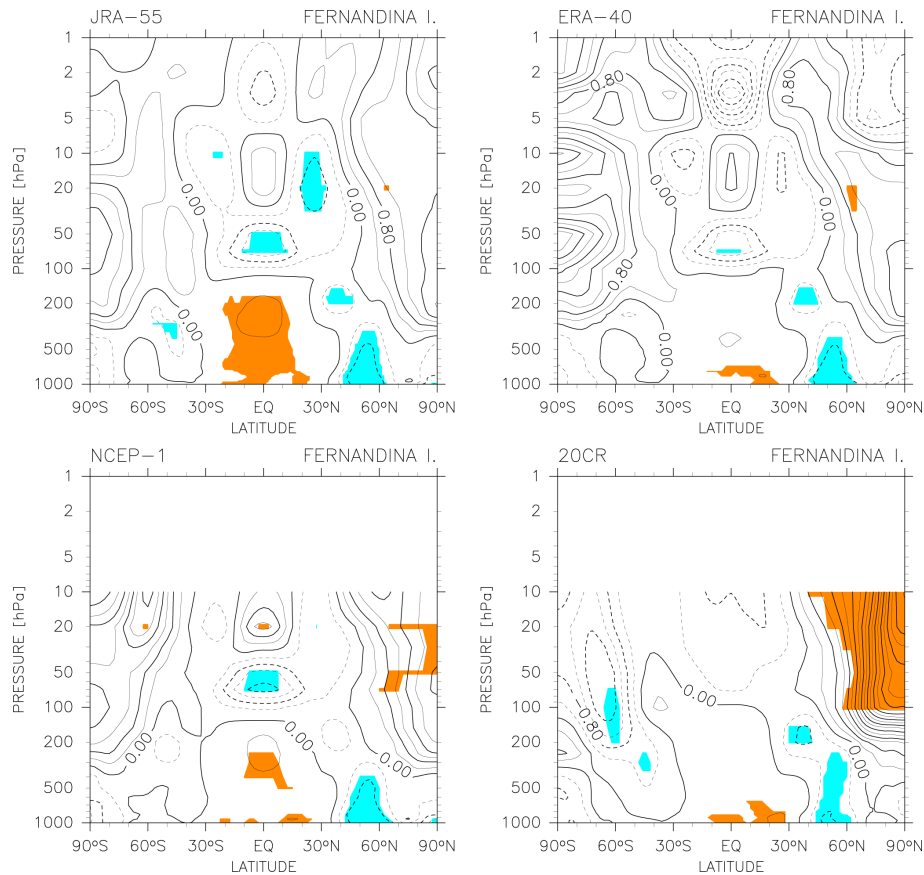
Figure 10. As in Fig. 8 but for the Fernandina Island eruption in June 1968.